Hindawi Publishing Corporation
Advances in Materials Science and Engineering
Volume 2016, Article ID 5973467, 10 pages
http://dx.doi.org/10.1155/2016/5973467

Research Article

Mechanical Performance and Chloride Diffusivity of Cracked RC Specimens Exposed to Freeze-Thaw Cycles and Intermittent Immersion in Seawater

Bei Shen,[1] Yinghua Ye,[1] Bo Diao,[1,2] and Xiaoning Zheng[1,2]

[1]*School of Transportation Science and Engineering, Beihang University, Beijing 100083, China*
[2]*State Laboratory of Subtropical Building Science, South China University of Technology, Guangzhou 510640, China*

Correspondence should be addressed to Bo Diao; diaobo@buaa.edu.cn

Received 14 June 2016; Revised 15 August 2016; Accepted 4 September 2016

Academic Editor: Robert Cerný

The effects of crack width on chloride ingress and mechanical behavior of reinforced concrete (RC) specimens were experimentally studied after exposure to 300 cycles of freeze-thaw and seawater immersion (75 times). Cracks were induced prior to exposure by an eccentric compression load which was sustained until the end of the exposure period. The maximum cracks widths induced in the four column specimens were 0, 0.06, 0.11, and 0.15 mm, respectively. Results show that when the crack width was less than 0.06 mm, the effect of cracks on chloride ingress could be neglected. However, when the crack width was more than 0.11 mm, chloride ingress was accelerated. Results of static loading tests show that both yield load and ultimate load of RC columns decreased as crack width increased. When the crack width was 0.15 mm, yield load and ultimate load of RC column specimen decreased by 17.0% and 18.9%, respectively, compared to a specimen without cracks. It was concluded that crack width significantly promoted local chloride ingress and mechanical performance degradation of RC structures in cold coastal regions or exposed to deicing salts.

1. Introduction

In actual service conditions it is common that concrete structures exhibit cracks and for exposure in a chloride-laden environment this will impair the structural performance.

Existing literature proves that in a marine environment the presence of crack accelerates chloride transport. Wang and Zhang [1] developed a numerical procedure to simulate chloride ingress in cracked concrete. It was found that, with increasing crack width, crack depth, and number of cracks, chloride ingress increased. However, the effect of loadings and stress on the chloride diffusion coefficient was not taken into account. Şahmaran [2] exposed RC beams exhibiting flexural cracks with different widths to a NaCl solution. The results revealed that the apparent chloride diffusion coefficient remained almost constant when the crack width was between 0.0294 and 0.1029 mm. In addition, X-ray diffractograms of the cracked concrete surface identified that the formation of calcite ($CaCO_3$) had resulted in self-healing. The diffusion coefficient increased rapidly when the crack width exceeded 0.135 mm. Li [3] utilized spray of NaCl solution (3.5% by weight) to simulate tidal and splash zones in marine environment. The effects of different cracking conditions (cracks induced by a sustained load or loaded to cracking and then released) and different crack widths (0.05, 0.1, and 0.2 mm) on corrosion initiation of steel bars were experimentally studied. It was found that when crack widths were less than 0.1 mm, the cracks demonstrated self-healing and the effect of cracks on chloride penetration was limited. However, when crack widths exceeded 0.1 mm, chloride penetration was accelerated. Win et al. [4] applied a bending load in concrete specimens to induce cracks in concrete specimens having widths of 0.1, 0.2, 0.3, and 0.5 mm, respectively. Then the specimens were exposed to a NaCl solution for 1 month. It was found by Electron Probe Microanalysis that the chloride penetration profile around the crack was more than twice that in the uncracked surface. Gowripalan et al. [5] immersed concrete prisms in 3% NaCl solution for 300 days. It was clearly observed that chloride diffusion coefficients of concrete under tension were higher than that of concrete

under compression. Wang et al. [6] applied flexural loads to RC beams and the loads were maintained. Then the RC beams were exposed to an accelerated salt fog (5% by weight NaCl) environment. The results showed that the chloride profile and the apparent chloride diffusion coefficient increased with the increase of the flexural loads. Cheewaket et al. [7] investigated the compressive strength and chloride diffusivity of concrete specimens exposed to seawater for 3, 4, 5, 7, and 10 years. The results showed that fly ash contributed to a better resistance to chloride ingress and steel corrosion; however fly ash lowered the 28-day compressive strength of concrete. Kwon et al. [8] investigated chloride diffusivity of wharves exposed to a coastal environment and developed a crack effect model to predict the service life of cracked concrete. Alkam and Alqam [9] predicted the service life of a reinforced concrete column exposed to a severe chloride environment. The study was based on chloride diffusion simulation in a concrete column during its anticipated life span. However, the mechanical behavior of column was not considered.

Increased chloride diffusivity of the concrete in the cover zone will result in accelerated corrosion initiation time of steel. Jaffer and Hansson [10] submerged beams with bending cracks in chloride solution (3% chloride content) for 2 weeks and subsequently dried the beams during the 2 weeks, which was repeated for 18 months. The results indicated that reinforcement corrosion occurred only at intersections of the rebar with cracks in the concrete cover. Furthermore, the observed depth loss due to pitting corrosion occurring at the cracks was greater than that calculated from average current densities. Poupard et al. [11] investigated steel corrosion in a RC beam after exposure to a tidal marine environment for 40 years. The results indicated that diameter loss of steel in the tension zone was about 30% whereas the diameter loss of steel in the compression zone did not exceed 2%. It indicated that microcracking resulting from tensile stresses increased both chloride and oxygen penetration which accelerated steel corrosion.

Many studies apply electrochemical corrosion methods to accelerate the steel corrosion process and focus on a relationship between amount of steel corrosion and loss of load-bearing capacity (Yoon et al. [12]; Torres-Acosta et al. [13]; Malumbela et al. [14]). Despite the fact that an electrochemical corrosion method is quick and convenient, with this method predominantly uniform corrosion attack over the steel surface will occur.

In contrast, in cracked RC structures in an aggressive environment, the corrosion process will be characterized by local pitting corrosion. Thus, steel corrosion processes induced by an electrochemical corrosion method are not comparable to real steel bars corrosion processes in RC structures exposed to an aggressive environment.

According to these studies, both cracks and tension stress increase chloride diffusivity and subsequently reduce time to corrosion initiation. Diao et al. [15] considered the effect of air content (3.2% and 6.1%). The results showed that the yield load, as well as the ultimate load, and the ductility of RC beams with higher air content increased after the combined action of freeze-thaw cycles and seawater immersion. Liu et al. [16] experimentally studied the effects of seawater corrosion and freeze-thaw cycles on the structural behavior of fatigue damaged reinforced concrete (FDRC) beams. The results showed that when the FDRC beams were exposed to an environment of alternate exposure to freeze-thaw and seawater immersion, a more rapid reduction in the strength and stiffness of the beams was observed. It is therefore concluded that comparative studies on loss of performance due to degradation and chloride diffusivity of RC structures are lacking in the existing literature and only a limited number of the studies consider the combined effect of freeze-thaw cycles, seawater immersion, and crack width on RC structures.

Table 1: Proportions of concrete mixture.

Concrete composition	
Water (kg/m^3)	184
425 Portland cement (kg/m^3)	460
River sand (kg/m^3)	609
Coarse aggregates (kg/m^3)	1130
Fly ash (kg/m^3)	53
Water-reducing admixtures (kg/m^3)	4.18
Air-entraining admixtures (mL/m^3)	98.6

Note: 425 Portland cement refers to a cement class in China; its compressive strength at age of 28 d was 42.5 MPa.

This paper reports on laboratory experiments on combined effects of crack width, freeze-thaw cycles, and seawater immersion performed on RC column specimens. In this study, cold coastal environment or deicing conditions were simulated by alternate action of freeze-thaw cycles and seawater immersion. Different cracks were induced in RC specimens by sustained eccentric compression load and the maximum cracks widths achieved in the specimens ranged from 0.0 to 0.15 mm. During a period of freeze-thaw cycles alternated with seawater immersion, the evolution of cracks was monitored. After alternate exposure conditions consisting of 300 cycles of freeze-thaw and seawater immersion (75 times), a static loading test and the determination of chloride profiles were conducted. Furthermore, the effect of crack width on chloride diffusivity was analyzed. This study combined measurements related to chloride transport properties and to mechanical performance in a single experiment which distinguished it from other studies referenced in the paper.

2. Experimental Details

2.1. Specimens. The specimens used in the current study included RC column specimens and plain concrete prism specimens. The plain concrete specimens were used to determine compression strength of concrete whereas RC column specimens were used to investigate chloride diffusivity and deterioration of structural performance. The details of the concrete mixture are listed in Table 1. The water-cement ratio was 0.40.

All specimens (column and plain concrete) were made from one batch of concrete. The air content in the current concrete mixture was measured with the pressure method according to the standard test method for air content of

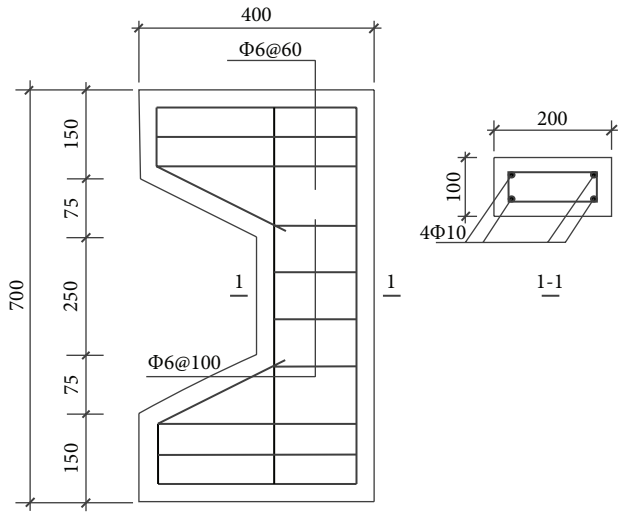

Figure 1: Reinforcement arrangement and dimensions of column specimens.

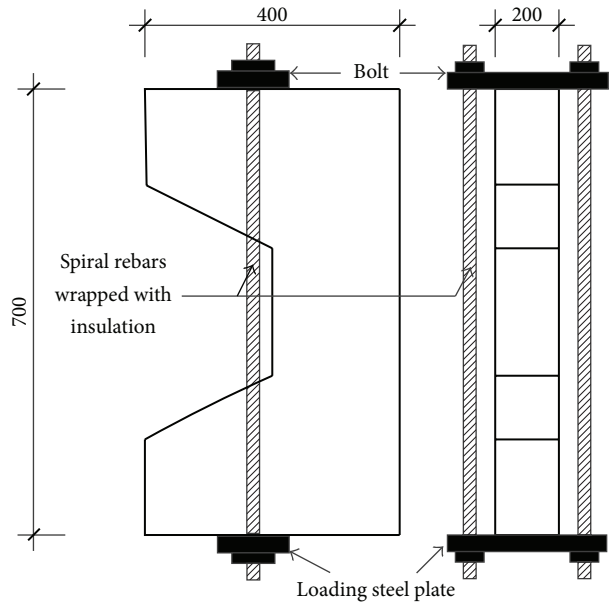

Figure 2: Sustained loading system to induce cracks.

freshly mixed concrete (ASTM C231/C231M). The air content amounted to 5.7%. The average compressive strength of the concrete used for the five RC column specimens was 41 MPa, as determined on the prisms at an age of 28 days.

Figure 1 shows details of the reinforcement arrangement and dimensions of the RC column specimens. Five RC column specimens were made, denoted by COL-0 to COL-4. All five column specimens were designed with 700 mm height and with a rectangular cross section of $b \times h = 100 \times 200$ mm, as shown in Figure 1. The thickness of the concrete cover was 30 mm. Four round plain bars with 10 mm diameter were symmetrically placed as longitudinal bars. The longitudinal bars had yield and ultimate strengths of 510 and 825 MPa, respectively. All specimens were demolded 24 hours after casting and thereupon cured under standard temperature and moisture conditions. At the age of 23 days, except for specimen COL-0 (no freeze-thaw, no chloride), the remaining four column specimens were immersed in seawater for 4 days. At the age of 28 d, different crack widths were induced in RC column specimens COL-1 up to COL-4. Then specimens COL-1 up to COL-4 were put into the temperature control chamber for freeze-thaw cycling. Column specimen COL-0 was exposed to an atmospheric environment and was regarded as the reference.

2.2. Cracks in RC Column Specimens. At the age of 28 d, different flexural cracks were induced by an eccentric compression load applied on RC column specimens COL-1 up to COL-4. The eccentric compression load was applied on these four column specimens by tightening the bolts attached to the spiral rebar passing through the brackets at two ends of the column, as illustrated in Figure 2. The eccentricity of the eccentric compression load was 130 mm. The prespecified widths of the resulting flexural cracks were controlled by the level of the applied eccentric compression load.

The resulting crack widths were quantified by a Crack Width Measuring Instrument (optical microscope). The maximum flexural cracks widths of 0.0, 0.06, 0.11, and 0.15 mm were induced to RC column specimens COL-1, COL-2, COL-3, and COL-4, respectively. For all column specimens, the maximum crack width was denoted as w_m and listed in Table 2. The maximum crack width was designed to be basically equivalent to that occurring under normal service conditions.

Table 2: Test conditions of reinforced concrete column specimens.

Group	COL-0	COL-1	COL-2	COL-3	COL-4
Max crack width w_m (mm)	0	0	0.06	0.11	0.15
Environment simulation	No	Yes	Yes	Yes	Yes
Number of freeze-thaw cycles	0	300	300	300	300
Number of times of immersion in seawater	0	75	75	75	75
Age at static loading (day)	103	103	103	103	103

2.3. Environment Simulation of Freeze-Thaw Cycles and Seawater Immersion. In this study, all tests were performed in the Civil Engineering Laboratory at Beihang University in Beijing. The environment simulation of cold coastal regions or deicing conditions included 75 cycles of alternate exposure. During 1 cycle of alternate exposure, the column specimens were placed in a temperature controlled chamber without exposure to chlorides for 4 cycles of freeze-thaw (16 h), and thereupon the column specimens were completely immersed (over the full height) in seawater solution for 8 h. Each freeze-thaw cycle lasted 4 h, with 2.5 h of freezing and 1.5 h of thawing. The freeze-thaw cycles were simulated according to

the fast freeze method described in experimental methods of long-term properties and durability of normal concrete (GB/T 50082-2009) [17]. The internal temperature at the center of a concrete specimen was monitored by an embedded temperature sensor. The maximum and minimum internal temperature during a freeze-thaw cycle were 8 ± 2°C and −15±2°C, respectively. During immersion the temperature of the seawater ranged between 15°C and 20°C. The environment simulation of the alternate exposure started at an age t_1 = 28 d and ended at t_2 = 103 d. The total duration of the alternate exposure amounted to 75 days. The seawater was an artificially mixed solution of 3% (by weight) sodium chloride (NaCl) and 0.34% (by weight) magnesium sulfate ($MgSO_4$).

Details on the environment simulation and maximum crack width in column specimens are shown in Table 2. The eccentric compression load was maintained to keep the cracks open until the end of 75 cycles of alternate exposure.

The evolution of all crack widths was monitored during the 75 cycles of alternate exposure. In order to minimize the impact of environmental conditions, the sustained loading system was covered with waterproof material and insulations, as shown in Figure 2. For column specimens COL-2 to COL-4, the sustained eccentric compression loads were removed after 75 cycles of the alternate exposure. Then the static loading tests were conducted on specimens COL-0~COL-4 until failure followed by determination of the chloride profiles.

2.4. Static Loading Test. Figure 3 shows the scheme of the static loading test. The RC column specimens COL-0~COL-4 were supported by a hinged support at both ends of a column specimen. The lateral displacements of the column specimen were measured by three displacement sensors. Strains in longitudinal bars and concrete were measured by wire strain gauges prepared before the loading test. The eccentricity between the loading jack and column specimens was 130 mm.

2.5. Chloride Content Test

2.5.1. Method for Chloride Content Test. After the static loading test, cylindrical samples were drilled from column specimens COL-0~COL-4, as shown in Figure 4. For each column specimen, 7 cylindrical samples were retrieved from the tensile side of a column specimen, which included both cracked and uncracked samples. The cores having a diameter of 50 mm and a depth of 30 mm were drilled evenly distributed over the height. Each core was then subdivided along the depth to obtain 3 slices having a thickness of 10 mm. Each slice was ground into a fine powder to quantify the free chloride content. The coarse aggregates were sifted from a slice when the slice was ground into fine powder. The free chloride was extracted by distilled water at room temperature. For all slices, powder was taken from each slice and dissolved in distilled water to prepare the sample solution. The free chloride content in each ground slice was determined by the Ion Selective Electrode Method according to the standard JTJ 270-98 [18]. Based on the measured chloride profile of each sample, the value of the apparent chloride diffusion coefficient D_a was determined by regression analysis using (2) as to result into the best fit curve. In this study, the

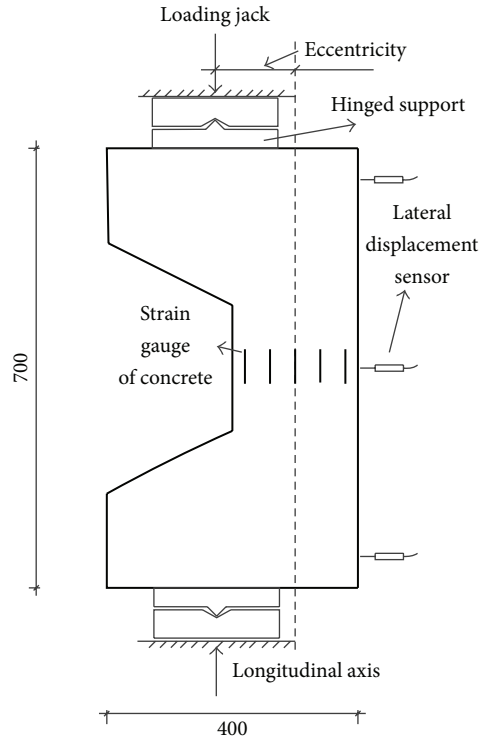

Figure 3: Scheme of static loading test.

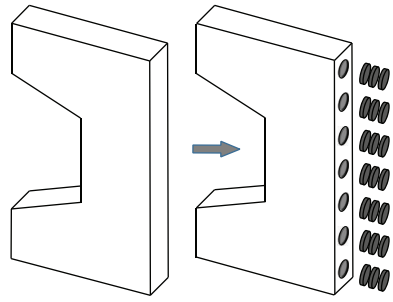

Figure 4: Sampling of concrete along the tension side of column specimens.

chloride diffusivity of column specimens COL-1~COL-4 was determined by analysis of the measured chloride profile and eventually characterized by the apparent chloride diffusion coefficient D_a.

2.5.2. Calculation of Time to Corrosion Initiation. To evaluate the effect of chloride diffusivity on RC column specimens, time to corrosion initiation was calculated based on the apparent chloride diffusion coefficient D_a. In general, during the service life the chloride content at the steel surface should not exceed the critical chloride content [8]. Thus, in this study, it is assumed that time to corrosion initiation T was reached when the chloride content at the steel surface has reached the critical chloride content C_{cr}. In this study for the critical chloride content causing initiation of steel corrosion C_{cr} = 0.07% has been adopted as found in a study of Oh [19] in

which similar aggressive environment was considered. C_{cr} related to free chloride and was expressed by mass of binder.

In order to calculate the chloride profile resulting from ingress of penetrating chlorides, Collepardi et al. [20] assume chloride diffusion into concrete to be one-dimensional non-steady state in a semi-infinite medium, following Fick's second law, generally expressed by

$$\frac{\partial C}{\partial t} = D\frac{\partial^2 C}{\partial x^2}, \tag{1}$$

where C is the chloride content at depth x after an exposure period t. D is the apparent chloride diffusion coefficient which is considered to remain constant during the complete exposure period.

Assuming that the initial and boundary conditions are $C(x = 0, t) = C_s$ and $C(x, t = 0) = 0$, respectively, the analytical solution to (1) is given by (2), that is, the so-called error function (erf) solution as described in Crank [21].

$$C = C_s - (C_s - C_i) \cdot \operatorname{erf}\left(\frac{x}{2\sqrt{D \cdot t}}\right), \tag{2}$$

where C_s is surface chloride content and C_i is initial chloride content.

The chloride diffusion coefficient decreased as exposure time increased in service life because of continued cement hydration. To take this ageing effect into account, Tang and Nilsson [22] utilize (3) to describe the development of the chloride diffusion coefficient over time.

$$D_t = D_{\text{ref}}\left(\frac{t_{\text{ref}}}{t}\right)^m, \tag{3}$$

where D_t is chloride diffusion coefficient at time t, D_{ref} is the chloride diffusion coefficient at reference time t_{ref} ($t_{\text{ref}} = 28$ d), and m is the so-called ageing factor. Following the Chinese standard for durability assessment of concrete structures (CECS220:2007) [23] in this study $m = 0.3$ is adopted for the concrete mixture used.

$$\begin{aligned} D_t &= D_{\text{ref}}\left(\frac{t_{\text{ref}}}{t}\right)^m, \quad t < t_R, \\ D_t &= D_{\text{ref}}\left(\frac{t_{\text{ref}}}{t_R}\right)^m, \quad t \geq t_R, \end{aligned} \tag{4}$$

where t_R is the time after which the diffusion coefficient is assumed to remain constant and t_R is generally assumed to be 30 years [24].

D_t is a function of time that cannot be directly put into the error function solution without time integration. Tang and Gulikers [25] substitute (4) into (5) to integrate I. Consequently, I can be expressed by (6) and (7). As given in Figure 5, t_1 is the start of exposure period and t_2 is the end of exposure period.

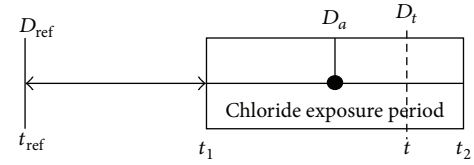

Figure 5: The scheme of exposure time.

$$I = \int_{t_1}^{t_2} D_t\, dt, \tag{5}$$

$$I = \frac{D_{\text{ref}} \cdot t_{\text{ref}}^m}{1 - m} \cdot \left(t_2^{1-m} - t_1^{1-m}\right), \quad t_2 < t_R, \tag{6}$$

$$I = D_{\text{ref}} \cdot \left[\frac{t_{\text{ref}}^m \cdot \left(t_R^{1-m} - t_1^{1-m}\right)}{1 - m} + \left(\frac{t_{\text{ref}}}{t_R}\right)^m (t_2 - t_R)\right], \quad t_2 \geq t_R. \tag{7}$$

For each sample the measured chloride profile is used to obtain surface chloride content C_s and apparent chloride diffusion coefficient D_a by regression analysis yielding the best fit curve. By substituting (3) into (5), the reference value D_{ref} can then be calculated using

$$D_a = \frac{\int_{t_1}^{t_2} D_{\text{ref}}\left(t_{\text{ref}}/t\right)^m dt}{\int_{t_1}^{t_2} dt}. \tag{8}$$

By substituting I for $D \cdot t$ in (2) to obtain (9), the time dependence of the chloride diffusion coefficient could be considered.

Based on C_s and D_{ref} obtained for each sample, substituting for the critical chloride content $C_{cr} = 0.07\%$, concrete cover $x = 30$ mm, $t_1 = t_{\text{ref}} = 28$ d, $t_R = 30$ year, $C_i = 0.007\%$, and $m = 0.3$ into (9), the magnitude of I could be calculated. $C_i = 0.007\%$ was obtained on samples retrieved from specimen COL-0. Next, the time to corrosion initiation T can be calculated by (10) and (11) which are derived from (6) and (7).

$$C_{\text{cr}} = C_s - (C_s - C_i) \cdot \operatorname{erf}\left(\frac{x}{2\sqrt{I}}\right), \tag{9}$$

$$T = \left[\frac{1 - m}{D_{\text{ref}} t_{\text{ref}}^m} \cdot I + t_1^{1-m}\right]^{1/(1-m)}, \quad T < t_R, \tag{10}$$

$$T = t_R + \left(\frac{t_R}{t_{\text{ref}}}\right)^m \left[\frac{I}{D_{\text{ref}}} - \frac{t_{\text{ref}}^m \left(t_R^{1-m} - t_1^{1-m}\right)}{1 - m}\right], \quad T \geq t_R. \tag{11}$$

3. Results and Discussion

3.1. Monitoring Results during Environment Simulation

3.1.1. Crack Evolution under Chloride Environment. As previously mentioned, a sustained eccentric compression load

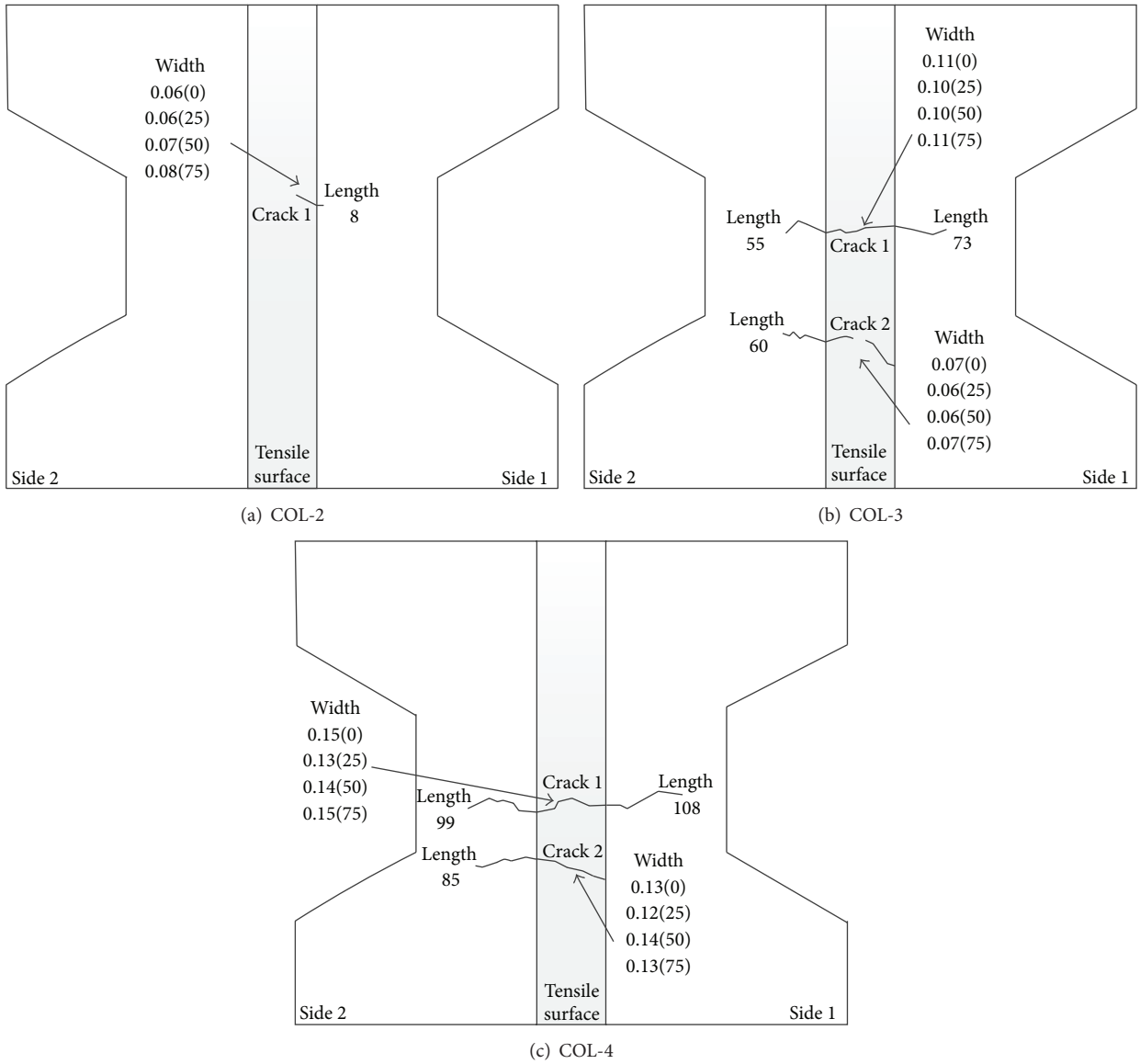

Figure 6: Distribution and development of cracks in COL-2~COL-4 after a specified number of series of cyclic exposure.

was applied to column specimens COL-2~COL-4 to induce and maintain cracks. As expected, the cracks were distributed on the tensile surface of the column specimens. In the case of COL-3 and COL-4, the main cracks extended from the tensile surface to two sides of the cross section and extended beyond the concrete cover depth. As shown in Figure 6, the evolution of cracks in column specimens COL-2, COL-3, and COL-4 was monitored after 0, 25, 50, and 75 series of cyclic exposure. The mechanical load was maintained during the complete period of exposure to freeze-thaw cycles and seawater immersion. During 75 series of cyclic exposure, the crack width remained constant.

3.1.2. Self-Healing Effect of Cracks. Figure 7 shows a picture of Crack 1 in column specimen COL-2, Crack 2 in COL-3, and Crack 2 in COL-4 after 75 series of alternate action, that is, at the end of the exposure period at an age of 103 days. As can be observed from Figure 7, white traces along Crack 1 in COL-2 and Crack 2 in COL-3 were clearly visible whereas the white traces were not evident at Crack 2 in COL-4. The study of Şahmaran [2] indicated that the white deposit formed by calcite ($CaCO_3$) contributed to a self-healing effect of concrete cracks, which was responsible for the blockage of transportation processes along the crack path. In other words, for small crack widths, such as Crack 1 in COL-2 and Crack 2 in COL-3, a self-healing effect of cracks was observed and the white deposit impeded the chloride transport process during the period of environment simulation of freeze-thaw cycles and seawater immersion. However, for larger crack widths, such as Crack 2 in COL-4, the self-healing effect of crack was not observed.

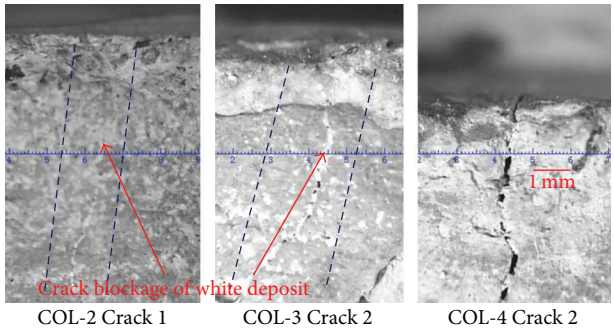

FIGURE 7: Self-healing effect of cracks after 75 rounds of alternate exposure.

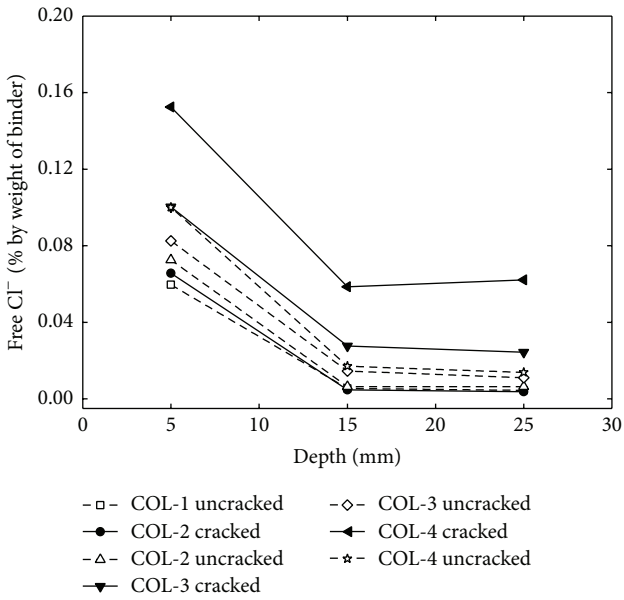

FIGURE 8: Measured chloride profiles of uncracked and cracked concrete surfaces of column specimens.

3.2. Results and Analysis of Chloride Diffusivity

3.2.1. Chloride Content of Uncracked and Cracked Concrete. For comparison, the average free chloride content in uncracked and cracked concrete parts of column specimens COL-1~COL-4 is plotted in Figure 8. For uncracked concrete parts, represented by dashed lines in Figure 8, the chloride content at each depth is an average value of uncracked samples on the same column specimen. For cracked concrete parts, represented by solid lines in Figure 8, the chloride content at each depth is an average value of cracked samples on the same specimen. For all chloride profiles, when the depth was more than 10 mm, the chloride content changed little as the depth increased.

As shown in Figure 8, the chloride content of cracked concrete was similar to the chloride content in uncracked concrete for column specimen COL-2 (w_m = 0.06 mm). This could be attributed to the self-healing effect observed in Figure 7. The white deposit blocked the flow path of crack and consequently impeded the chloride penetration according to the study of Şahmaran [2].

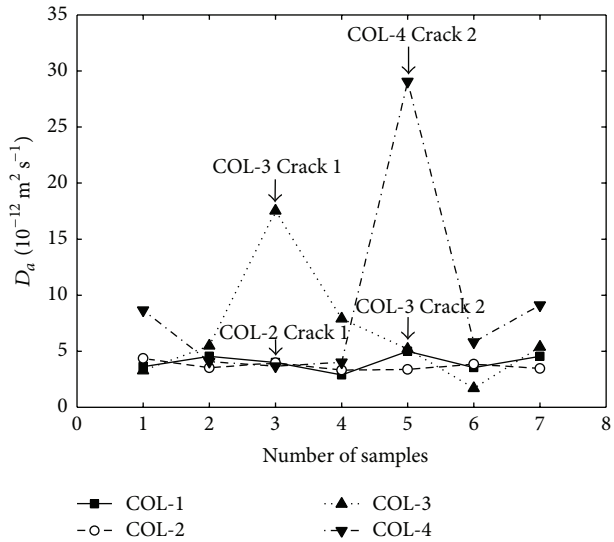

FIGURE 9: Chloride diffusion coefficient of all samples of column specimens.

For column specimens COL-3 (w_m = 0.11 mm) and COL-4 (w_m = 0.15 mm), the chloride contents of cracked concrete were larger than the chloride contents of uncracked concrete. This finding implies that the chloride diffusivity of column specimens was accelerated when w_m was larger than 0.11 mm.

3.2.2. Chloride Diffusivity of Uncracked and Cracked Concrete. The apparent chloride diffusion coefficients D_a of seven samples of all specimens COL-1~COL-4 are given in Figure 9. As shown in Figure 9, the apparent chloride diffusion coefficients in cracked concrete are higher than those in uncracked concrete. The apparent chloride diffusion coefficients D_a obtained on uncracked and cracked concrete parts of column specimens COL-1~COL-4 are shown in Figure 10 for comparison. For uncracked concrete parts of specimens COL-1~COL-4, represented by dashed lines in Figure 10, the apparent chloride diffusion coefficient is an average of uncracked samples in the same specimen.

From Figures 9 and 10, it is can be deduced that D_a in cracked concrete increased as crack width increased. When the crack width was less than 0.06 mm, the difference between average D_a values in cracked and uncracked concrete was minor. When the crack width exceeded 0.11 mm, the average D_a in cracked concrete increased drastically. For column specimen COL-4, D_a in cracked concrete (29.06×10^{-12} m^2/s) was 4.93 times D_a of uncracked concrete (5.89×10^{-12} m^2/s). Moreover, D_a in Crack 2 of specimen COL-4 (29.06×10^{-12} m^2/s) was 7.23 times the average D_a of uncracked specimen COL-1 (4.02×10^{-12} m^2/s). It is concluded that the wider cracks expedited the chloride penetration significantly.

Although the concrete was visually uncracked, the average D_a increased from COL-1 to COL-4. What is more, D_a in uncracked concrete of COL-4 (5.89×10^{-12} m^2/s) was

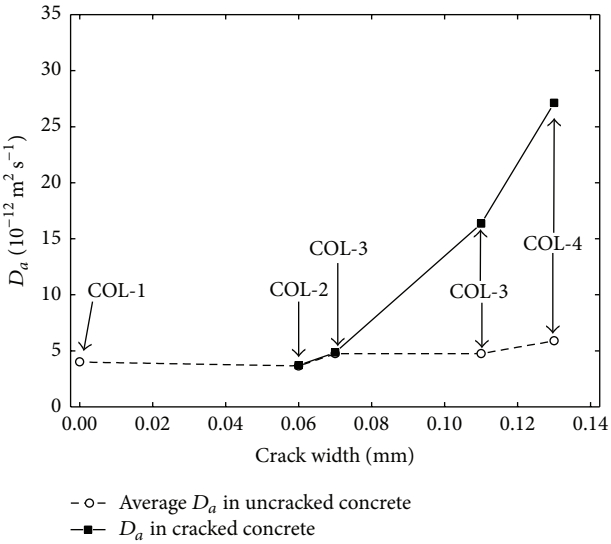

Figure 10: Chloride diffusion coefficient of uncracked and cracked concrete of column specimens.

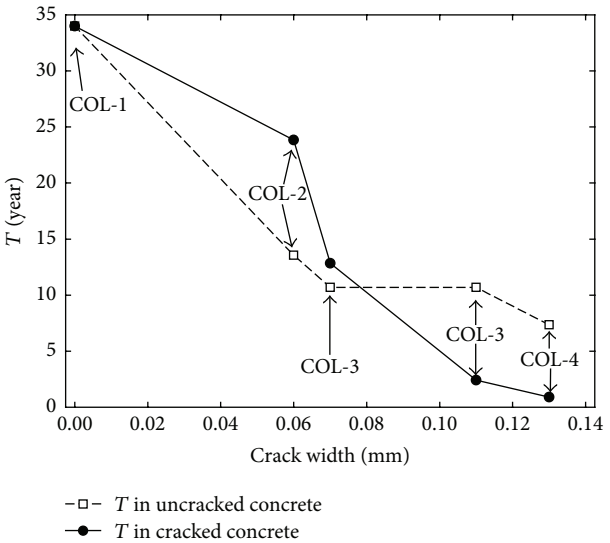

Figure 11: Time to corrosion initiation of uncracked and cracked concrete of column specimens.

1.47 times the average D_a of the unloaded column specimen COL-1 (4.02×10^{-12} m^2/s). A possible explanation is that the sustained mechanical load generated microcracking in the concrete tension zone and microcracking increased chloride diffusivity. In the study of Gowripalan et al. [5] the same explanation was given.

3.2.3. Predicted Time to Corrosion Initiation of Cracked RC Column Specimens. The calculated time to corrosion initiation T of both uncracked and cracked concrete of column specimens COL-1~COL-4 is shown in Figure 11 for comparison.

As can be seen from Figure 11, when the crack width was more than 0.11 mm, T decreased sharply and the difference between T values of uncracked and cracked concrete became larger. This is due to the fact the presence of cracks increased the chloride diffusion coefficient and consequently shortened the resulting time to corrosion initiation. It can be concluded that, for RC structures in service, the cracks had an adverse effect on time to corrosion initiation. The adverse effect of cracks depended on its width.

This study focused on the RC structures in cold coastal region or under deicing conditions. It was highlighted that different levels of service loads resulted in different crack widths of RC structures under alternate action of freeze-thaw cycles and seawater immersion, based on which the time to corrosion initiation was evaluated. The results could provide technical reference for durability design of reinforced concrete structures in cold coastal environment or under deicing conditions.

3.3. Results and Analysis of Static Loading Test. For all column specimens COL-0~COL-4 the failure mode of static eccentric compression loading was ductile failure of large eccentric compression, where tensile reinforcement bars yielded and then concrete in the compression zone crushed. During static loading, the cracks in specimens COL-2~COL-4, which were closed after the sustained load was removed, opened again and became the major cracks of eccentric compression failure. The static loading results are summarized in Table 3. As can be seen from Table 3, the yield load and ultimate load decreased as w_m increased, whereas the ductility coefficient δ_u/δ_y showed no obvious tendency. The ratio δ_u/δ_y indicates the deformation capacity of column specimens after yielding of longitudinal bars. The yield load and ultimate load of COL-4 (w_m = 0.15 mm) decreased by 17.0% and 18.9%, respectively, with COL-1 as reference. This implied that COL-4 could not satisfy the safety requirements. The results demonstrated that, under combined action of freeze-thaw cycles and seawater immersion, the presence of cracks had a significant impact on performance degradation of RC columns.

When the sustained load was applied, that is, at an age of 28 d, the column specimens already showed initial damage which had an adverse effect on mechanical performance. The 75 days of alternate exposure would accelerate the initial damage. What is more, the concrete strength decreased due to freeze-thaw cycles [15] and the presence of cracks would accelerate chloride ingress after depassivation steel corrosion. After 75 days of alternate exposure, corrosion was observed at intersections of the rebar with cracks. The degradation of concrete strength, corrosion of steel bar, and damage of preloading led to the loss of mechanical performance after combined action of alternate exposure and cracks.

The load-deflection curves of column specimens COL-0~COL-4 are shown in Figure 12. As can be seen from Figure 12, both the ultimate load and ductility of specimen COL-0 are maximum whereas the ultimate load and ductility of specimen COL-4 are minimum. For column specimens COL-0~COL-4, the ductility shows no clear trend.

Table 3: Summary of static loading test results on column specimens.

Specimen	w_m (mm)	Yield load (kN)	δ_y (mm)	Ultimate load (kN)	δ_p (mm)	δ_u (mm)	Ductility δ_u/δ_y
COL-0	0	174.3	2.76	185.0	4.06	5.81	2.11
COL-1	0	170.1	2.65	174.7	3.47	3.84	1.45
COL-2	0.06	160.2	3.11	171.6	3.76	5.94	1.91
COL-3	0.11	157.2	2.99	166.3	3.21	5.50	1.84
COL-4	0.15	141.2	3.11	141.7	3.22	3.27	1.05

Note: w_m: maximum crack width; δ_y: deflection at yield load; δ_p: deflection at ultimate load; δ_u: deflection at 85% of ultimate load on the descending portion of the load-deflection curve.

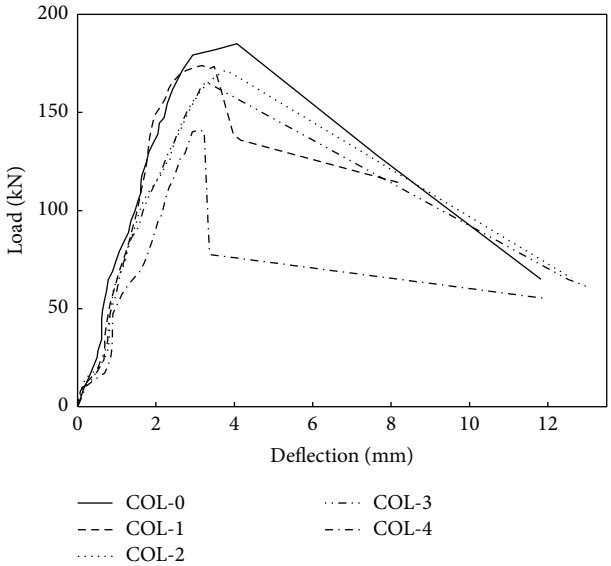

Figure 12: Load-deflection curves of column specimens.

4. Conclusions

In this study, cracked RC column specimens were continually exposed to an aggressive environment of freeze-thaw cycles and seawater immersion for 75 days. Following this exposure the static loading test was conducted on these specimens. After mechanical failure, RC column specimens were sampled for chloride profiling, and subsequently the chloride diffusion coefficient was calculated. This information was used to predict the time to corrosion initiation based on an assumed critical chloride content. Conclusions specifically related to the cracks are as follows:

(1) Different crack widths were induced on RC column specimens by a sustained load. After the exposure of 300 cycles of freeze-thaw and seawater immersion (75 times), the yield load and ultimate load of column specimen decreased as the maximum crack width increased. When the maximum crack width was 0.15 mm, compared to a RC column specimen without cracks, the yield load and ultimate load decreased by 17.0% and 18.9%, respectively, which means that the combined effect of freeze-thaw cycles, seawater immersion, and cracks on mechanical performance was considerable.

(2) Sustained load induced cracks in concrete. When the crack width was less than 0.06 mm, the effect of cracks on chloride ingress may be neglected. When the crack width exceeded 0.11 mm, cracks accelerated the chloride ingress.

(3) Based on calculated predictions, for RC structures in cold coastal region or under deicing conditions, the time to corrosion initiation decreased as crack width increased. When the crack width was more than 0.11 mm, a clear decline of time to corrosion initiation was obtained as a consequence of accelerated chloride diffusivity.

In this study, the durability of cracked column specimens was tested and evaluated from chloride ingress and mechanical performance. Both the number of specimens and chloride penetration depth after 75 days of alternate exposure were limited to allow for in-depth comparison and conclusions. Further studies will be performed to investigate the effect of cracks on mechanical performance and chloride penetration.

Notations

δ_y: Deflection at yield load
δ_p: Deflection at ultimate load
δ_u: Deflection at 85% of ultimate load on the descending portion of the load-deflection curve
D_a: Apparent chloride diffusion coefficients
w_m: Max cracks width.

Competing Interests

The authors declare that there is no conflict of interests regarding the publication of this paper.

Acknowledgments

This work was financially supported by the National Natural Science Foundation of China (Grant no. 51178020 and no. 51108015) and the Open Project of State Key Laboratory of Subtropical Building Science, South China University of Technology (2016ZA03).

References

[1] X. Y. Wang and L. N. Zhang, "Simulation of chloride diffusion in cracked concrete with different crack patterns," *Advances in Materials Science and Engineering*, vol. 2016, Article ID 1075452, 11 pages, 2016.

[2] M. Şahmaran, "Effect of flexure induced transverse crack and self-healing on chloride diffusivity of reinforced mortar," *Journal of Materials Science*, vol. 42, no. 22, pp. 9131–9136, 2007.

[3] C. Q. Li, "Corrosion initiation of reinforcing steel in concrete under natural salt spray and service loading-Results and analysis," *ACI Material Journal*, vol. 97, no. 6, pp. 690–697, 2000.

[4] P. P. Win, M. Watanabe, and A. Machida, "Penetration profile of chloride ion in cracked reinforced concrete," *Cement and Concrete Research*, vol. 34, no. 7, pp. 1073–1079, 2004.

[5] N. Gowripalan, V. Sirivivatnanon, and C. C. Lim, "Chloride diffusivity of concrete cracked in flexure," *Cement and Concrete Research*, vol. 30, no. 5, pp. 725–730, 2000.

[6] H. Wang, C. Lu, W. Jin, and Y. Bai, "Effect of external loads on chloride transport in concrete," *Journal of Materials in Civil Engineering*, vol. 23, no. 7, pp. 1043–1049, 2011.

[7] T. Cheewaket, C. Jaturapitakkul, and W. Chalee, "Concrete durability presented by acceptable chloride level and chloride diffusion coefficient in concrete: 10-year results in marine site," *Materials and Structures*, vol. 47, no. 9, pp. 1501–1511, 2014.

[8] S. J. Kwon, U. J. Na, S. S. Park, and S. H. Jung, "Service life prediction of concrete wharves with early-aged crack: probabilistic approach for chloride diffusion," *Structural Safety*, vol. 31, no. 1, pp. 75–83, 2009.

[9] M. K. Alkam and M. Alqam, "Prediction of the service life of a reinforced concrete column under chloride environment," *Advances in Materials Science and Engineering*, vol. 2015, Article ID 156298, 8 pages, 2015.

[10] S. J. Jaffer and C. M. Hansson, "The influence of cracks on chloride-induced corrosion of steel in ordinary Portland cement and high performance concretes subjected to different loading conditions," *Corrosion Science*, vol. 50, no. 12, pp. 3343–3355, 2008.

[11] O. Poupard, V. L'Hostis, S. Catinaud, and I. Petre-Lazar, "Corrosion damage diagnosis of a reinforced concrete beam after 40 years natural exposure in marine environment," *Cement and Concrete Research*, vol. 36, no. 3, pp. 504–520, 2006.

[12] S. Yoon, K. Wang, W. J. Weiss, and S. P. Shah, "Interaction between loading, corrosion, and serviceability of reinforced concrete," *ACI Structural Journal*, vol. 97, no. 6, pp. 637–644, 2000.

[13] A. A. Torres-Acosta, S. Navarro-Gutierrez, and J. Terán-Guillén, "Residual flexure capacity of corroded reinforced concrete beams," *Engineering Structures*, vol. 29, no. 6, pp. 1145–1152, 2007.

[14] G. Malumbela, M. Alexander, and P. Moyo, "Variation of steel loss and its effect on the ultimate flexural capacity of RC beams corroded and repaired under load," *Construction and Building Materials*, vol. 24, no. 6, pp. 1051–1059, 2010.

[15] B. Diao, J. Zhang, Y. Ye, and S. Cheng, "Effects of freeze-thaw cycles and seawater corrosion on the behavior of reinforced air-entrained concrete beams with persistent loads," *Journal of Cold Regions Engineering*, vol. 27, no. 1, pp. 44–53, 2013.

[16] Z. Liu, B. Diao, and X. Zheng, "Effects of seawater corrosion and freeze-thaw cycles on mechanical properties of fatigue damaged reinforced concrete beams," *Advances in Materials Science and Engineering*, vol. 2015, Article ID 536487, 15 pages, 2015.

[17] GB/T 50082-2009, *Experimental Methods of Long-Term Properties and Durability of Normal Concrete*, China Architectural & Building Press, Beijing, China, 2009 (Chinese).

[18] JTJ 270-98, "Testing code of concrete for port and waterwog engineering," Tech. Rep., China Communications Press, Beijing, China, 1998 (Chinese).

[19] B. H. Oh, S. Y. Jang, and Y. S. Shin, "Experimental investigation of the threshold chloride concentration for corrosion initiation in reinforced concrete structures," *Magazine of Concrete Research*, vol. 55, no. 2, pp. 117–124, 2003.

[20] M. Collepardi, A. Marcialis, and R. Turriziani, "Penetration of chloride ions into cement pastes and concretes," *Journal of the American Ceramic Society*, vol. 55, no. 10, pp. 534–535, 1972.

[21] J. Crank, *The Mathematics of Diffusion*, Clarendon Press, Oxford, UK, 2nd edition, 1975.

[22] L. P. Tang and L. O. Nilsson, "Chloride diffusivity in high strength concrete at different ages," *Nordic Concrete Research*, vol. 11, no. 1, pp. 162–171, 1992.

[23] CECS 220:2007, *Standard for Durability Assessment of Concrete Structures*, China Architectural & Building Press, Beijing, China, 2007 (Chinese).

[24] M. D. A. Thomas and E. C. Bentz, *Computer Program for Predicting the Service Life and Life-Cycle Costs of Reinforced Concrete Exposed to Chlorides*, Life365 Manual, SFA, 2002.

[25] L. P. Tang and J. Gulikers, "On the mathematics of time-dependent apparent chloride diffusion coefficient in concrete," *Cement and Concrete Research*, vol. 37, no. 4, pp. 589–595, 2007.